



CHORUS

This is the accepted manuscript made available via CHORUS. The article has been published as:

Measurement of the Electron-Antineutrino Angular Correlation in Neutron β Decay

G. Darius, W. A. Byron, C. R. DeAngelis, M. T. Hassan, F. E. Wietfeldt, B. Collett, G. L. Jones, M. S. Dewey, M. P. Mendenhall, J. S. Nico, H. Park, A. Komives, and E. J. Stephenson

Phys. Rev. Lett. **119**, 042502 — Published 25 July 2017

DOI: [10.1103/PhysRevLett.119.042502](https://doi.org/10.1103/PhysRevLett.119.042502)

Measurement of the electron-antineutrino angular correlation in neutron beta decay

G. Darius, W. A. Byron, C. R. DeAngelis, M. T. Hassan, and F. E. Wietfeldt

Tulane University, New Orleans, LA 70118

B. Collett and G. L. Jones

Hamilton College, Clinton, NY 13323

M. S. Dewey, M. P. Mendenhall, J. S. Nico, and H. Park*

National Institute of Standards and Technology, Gaithersburg, MD 20899

A. Komives

DePauw University, Greencastle, IN 46135

E. J. Stephenson

Indiana University, Bloomington, IN 47408

(Dated: June 12, 2017)

Abstract

We report the first result for the electron-antineutrino angular correlation (a coefficient) in free neutron beta decay from the aCORN experiment. aCORN uses a novel method in which the a coefficient is proportional to an asymmetry in proton time-of-flight for events where the beta electron and recoil proton are detected in delayed coincidence. Data are presented from a 15 month run at the NIST Center for Neutron Research. We obtained $a = -0.1090 \pm 0.0030(\text{stat}) \pm 0.0028(\text{sys})$, the most precise measurement of the neutron a coefficient reported to date.

PACS numbers: 13.30.Ce, 14.20.Dh, 23.40.-s

Precision measurements of the angular correlations in free neutron beta decay, and the neutron lifetime, determine the neutron decay axial vector (G_A) and vector (G_V) coupling constants. These give fundamental information about weak decays in the light quark sector. They are used to predict the rates of important charged weak interactions in nuclear and particle physics, astrophysics, and cosmology that involve a free neutron and proton, and provide sensitive tests of possible new physics beyond the Standard Model [1–3]. Key features of neutron decay are described by the formula of Jackson, Treiman, and Wyld [4], which gives the differential decay probability dN of a spin-1/2 beta decay system in terms of the angular correlations between the beta electron (\mathbf{p}_e) and antineutrino (\mathbf{p}_ν) momenta, and the neutron spin ($\boldsymbol{\sigma}$)

$$dN \propto 1 + a \frac{\mathbf{p}_e \cdot \mathbf{p}_\nu}{E_e E_\nu} + b \frac{m_e}{E_e} + \boldsymbol{\sigma} \cdot \left(A \frac{\mathbf{p}_e}{E_e} + B \frac{\mathbf{p}_\nu}{E_\nu} + D \frac{(\mathbf{p}_e \times \mathbf{p}_\nu)}{E_e E_\nu} \right). \quad (1)$$

Here E_e and E_ν are the electron and antineutrino energies. The parameters a , A , B , and D are correlation coefficients which are measured by experiment. Bloch and Møller [5] were the first to propose that the electron-antineutrino correlation, the a coefficient in Eq. 1, can be used to experimentally distinguish scalar (S), vector (V), axial vector (A), and tensor (T) currents in the weak interaction responsible for beta decay. This idea was famously used in the 1950s to demonstrate the V - A nature of the weak force [6]. In the Standard Model, the neutron a coefficient is given by [4]

$$a = \frac{1 - \lambda^2}{1 + 3\lambda^2}, \quad (2)$$

where $\lambda = G_A/G_V = -1.2723 \pm 0.0023$ [7]. The best current precision on λ comes from the beta asymmetry $A = -0.1184 \pm 0.0010$ [7–9] due to its much smaller relative uncertainty. The a and A coefficients have similar sensitivity to λ , and a has the feature that it is measured with an unpolarized neutron beam, so high precision neutron polarimetry is not needed. A key motivation for this work is that a precise comparison of the a and A coefficients is sensitive to new physics beyond the Standard Model, for example they depend differently on hypothetical scalar and tensor weak currents [10–12]. A significant reduction in the uncertainty of the neutron a coefficient will give (1) an improved value of λ ; (2) improved limits on scalar and tensor weak currents; (3) a sensitive test of the conserved-vector-current (CVC) hypothesis and improved limits on second-class weak currents [13]; and (4) eventually an improved determination of V_{ud} .

Previous neutron a coefficient experiments measured its effect on the shape of the recoil proton energy spectrum and were systematically limited at about 5% relative uncertainty [14–16]. The current accepted value is $a = -0.103 \pm 0.004$ [7]. aCORN is the first experimental realization of the novel “wishbone asymmetry” method first proposed by Yerozolimsky and Mostovoy [17–20]. When a neutron decays, the electron and recoil proton are transported by an axial magnetic field to a beta spectrometer on one end and a proton counter on the other. Electron and proton collimators restrict the transverse momenta of decay particles that reach their respective detectors. The decay region is surrounded by a 3 kV electrostatic mirror that reflects and preaccelerates decay protons toward the proton counter. The antineutrino is not detected, but conservation of energy and momentum restricts the antineutrino momentum into two similar groups, one correlated with the electron momentum and the other anticorrelated, such that the asymmetry in event rates is proportional to the a coefficient. See [21] for a more detailed description of the aCORN method and apparatus. A plot of proton time-of-flight (TOF) *vs.* beta energy for coincidence events forms a characteristic wishbone shape, shown in figure 1. The lower branch (group I) contains faster protons, where the electron and antineutrino momenta were correlated. The upper branch (group II) contains slower protons, where they were anticorrelated. For each slice of beta energy (E), we form the wishbone asymmetry $X(E)$ in the numbers of group I ($N^I(E)$) and group II ($N^{II}(E)$) events: $X(E) = (N^I(E) - N^{II}(E))/(N^I(E) + N^{II}(E))$. Using equation 1 and the calculated momentum acceptances for electrons and protons, it is straightforward to derive the following expression relating $X(E)$ to the a coefficient (see [21] for more details)

$$X(E) = af_a(E) [1 + \delta_1(E)] + \delta_2(E). \quad (3)$$

The geometric acceptance function $f_a(E)$ contains the momentum acceptances and the electron velocity. It depends on the axial magnetic field and collimator geometry and can be accurately calculated by Monte Carlo. There are two very small corrections. The first, $\delta_1(E)$, is a nonlinear geometric correction with a numerical value of -0.003 . The second, $\delta_2(E)$, results from the effect of the proton kinetic energy on the effective antineutrino acceptance; it has a numerical value of about $+0.0013$. Both $\delta_1(E)$ and $\delta_2(E)$ are calculated by Monte Carlo.

The aCORN experiment was installed and operated on the fundamental neutron physics end position NG-6 at the National Institute of Standards and Technology (NIST) Center for

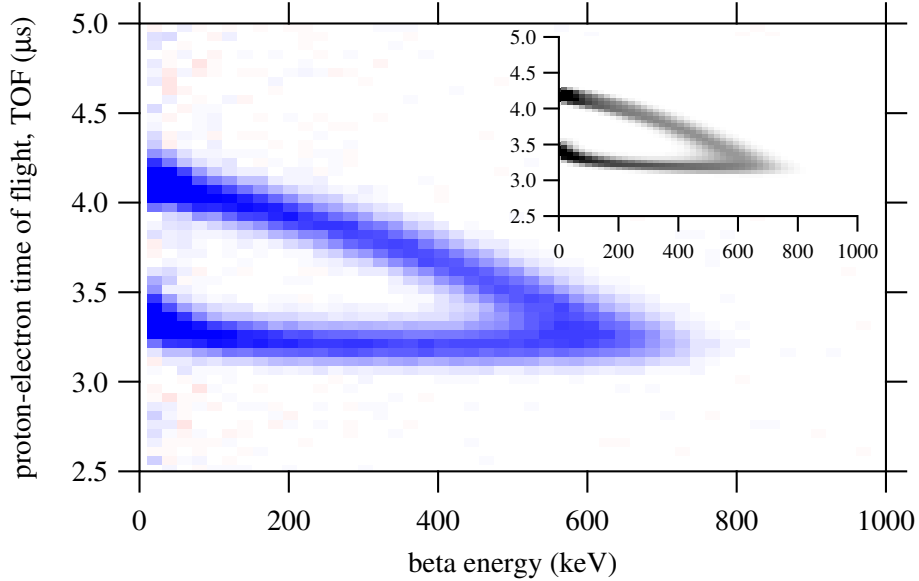


FIG. 1. The aCORN “wishbone” histogram plot of proton time of flight vs. beta energy for delayed coincidence neutron decay events. Blue pixels are positive and red are negative (due to the background subtraction). Inset: Monte Carlo simulation.

Neutron Research (NCNR) [22]. Figure 2 shows a diagram of the aCORN tower. The main magnet consists of 25 water-cooled pancake coils powered in series to produce a 36.2 mT axial magnetic field. Sets of 25 axial trim coils and 45 transverse trim coils, each independently served by computer-controlled current supplies, were used to reduce transverse magnetic fields to less than 0.004 mT in the electrostatic mirror and proton collimator.

The electrostatic mirror is a 0.25 mm wall PTFE cylindrical tube electroplated with 4.5 μm of copper on the inner surface [23, 24]. The copper is divided by etching into 63 electrically isolated horizontal bands and connected to a chain of 1.0 M Ω precision resistors to produce an approximately linearly varying electrostatic potential on the wall. At the top and bottom of the cylinder are wire grid planes (linear arrays of 100 μm wire, 2.0 mm spacing) held at ground and +3 kV, respectively. The axis of the neutron beam was located at potential +1.94 kV inside the mirror. The proton collimator is a 140 cm long monolithic aluminum tube with a series of 55 precision turned 8 cm diameter knife-edge apertures inside. Its length is such that all neutron decay protons make at least one full cycle of helical motion in the collimator. Below the electrostatic mirror is the beta collimator, a series of 17 tungsten plates, 0.5 mm thick with 5.5 cm diameter apertures, unevenly spaced to minimize

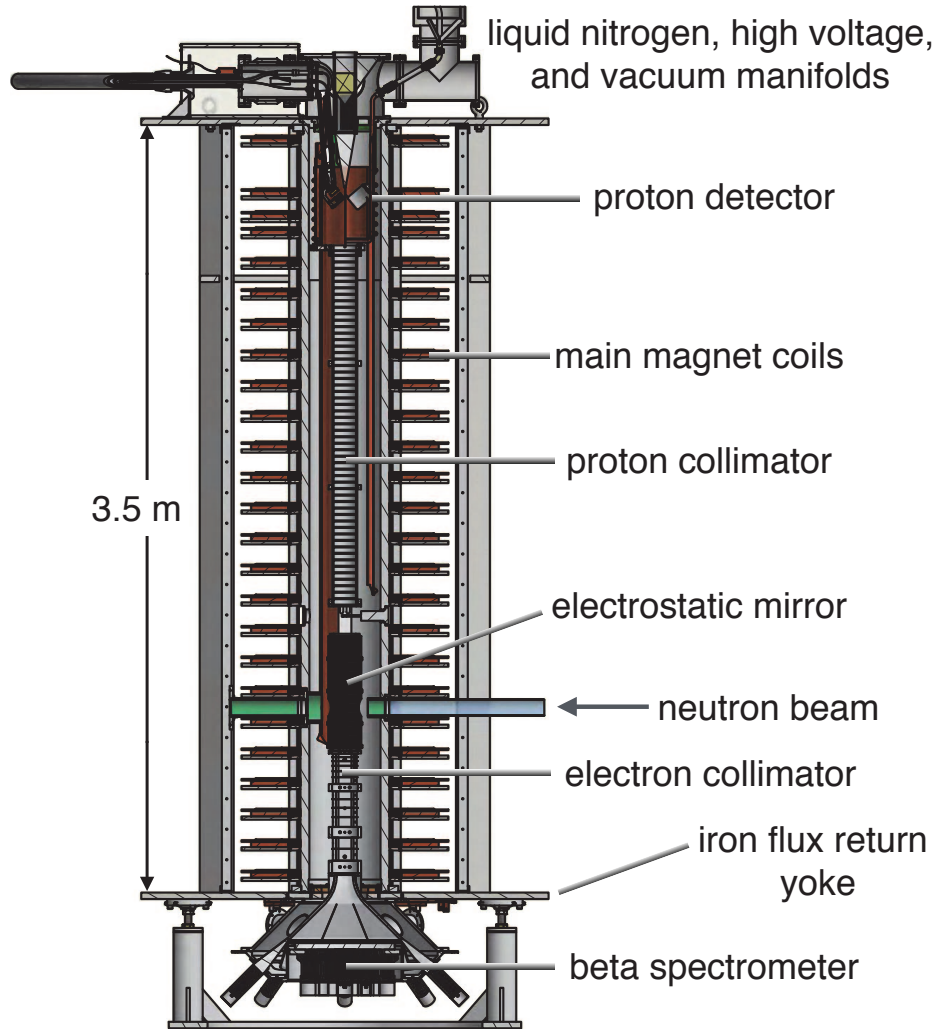


FIG. 2. A rendering of the aCORN apparatus indicating the major components and arrangement.

the number of scattered electrons that enter the beta spectrometer. The collimators and electrostatic mirror are attached to a rigid insert mount that is aligned to the magnet axis to within 10^{-4} radians. At the bottom of the tower is the backscatter suppressed beta spectrometer, described in more detail in another publication [25]. Electrons that pass the collimator are transported into the spectrometer and strike the energy detector, a 5 mm thick circular slab of Bicron BC-408 plastic scintillator, backed by an acrylic light guide and 19 7.6-cm hexagonal photomultiplier tubes (PMTs). Surrounding the energy detector is a tight circular array of 8 veto paddles; each consisting of a 10 mm thick BC-408 plastic scintillator blade, an acrylic light guide, and a 5.1-cm high-efficiency PMT. This veto array detects electrons that backscatter from the energy detector without depositing their full energy.

The energy response was linear from 100–1000 keV, and the energy resolution (FWHM) was measured to be 16.8 % (12.1 %) at 363 (975) keV. The backscatter veto efficiency was determined to be approximately 90% [25]. The proton counter is a 600 mm² liquid-nitrogen cooled silicon surface barrier detector held at a potential of -29 kV with a set of focusing electrodes. It is mounted slightly off axis so that electrons with upward trajectories cannot backscatter from it and subsequently reach the beta spectrometer. Pulses from the 19 energy PMTs, 8 veto PMTs, and the proton counter were digitized by a 100 MHz, 32 channel digitizing system PIXIE-16 [26] from which energy and timing signals were extracted for analysis. Additional details on the design, construction, alignment, and calibration of the aCORN apparatus and individual components are presented in previous publications [20, 21, 25].

The data set collected on NG-6 from February 2013 – May 2014, totalling 1900 beam hours, is presented here. Figure 1 shows the background subtracted and deadtime corrected wishbone plot from a typical data set (about 400 beam hours). Neutron beam-induced background was significant; the average coincidence signal to background ratio in the energy range of interest (100 – 360 keV) of the wishbone was 0.4. The data acquisition system was configured so that every electron signal that arrived within 10 μ s before or 1 μ s after each proton signal was treated as a separate event, which guaranteed that random coincidences associated with background had no time structure. Time-correlated background, due to for example neutron induced radioactivity, are expected to be negligible because 1) materials through which the neutron beam passes lack isotopes with decay lifetimes on the time scale of the coincidence window and 2) the proton and electron detectors are well separated in space. We tested for this in the data by fitting the off-wishbone background for each energy slice to a straight line and obtaining good fits with a distribution of slopes statistically consistent with zero. The energy calibration of the beta spectrometer was monitored every 2–3 days using a set of *in situ* conversion electron sources, typically ¹¹³Sn and ²⁰⁷Bi. These data were used to correct minor gain drifts within a data set. To obtain the final energy calibration of each data set, the wishbone energy spectrum (the wishbone histogram as in figure 1 summed over TOF and plotted *vs.* energy) was fit to the theoretical spectrum, shown in figure 3. The theoretical spectrum was calculated from the Fermi beta decay distribution with the aCORN transverse momentum cuts applied and convoluted with a Gaussian energy resolution function with width proportional to \sqrt{E} . Four parameters were

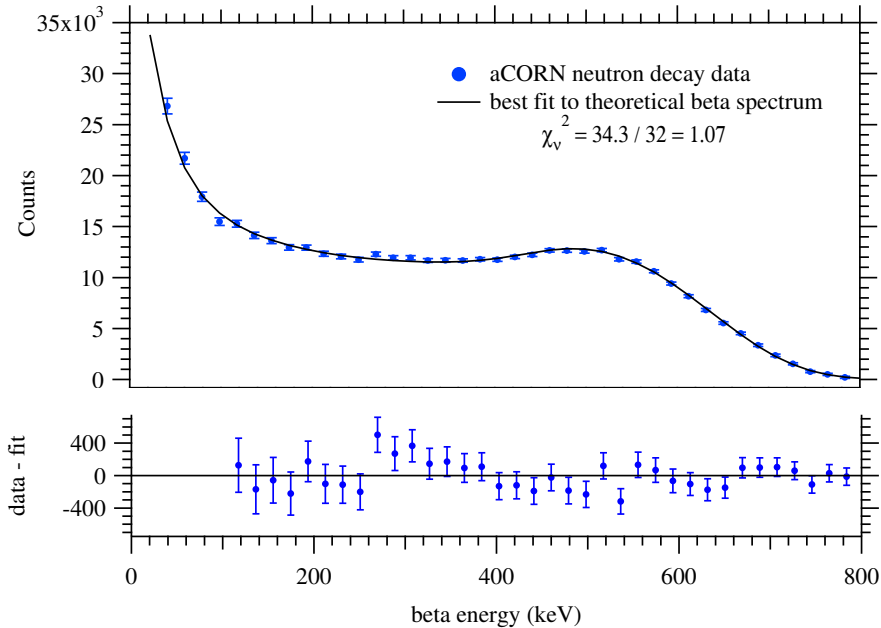


FIG. 3. Top: The wishbone energy spectrum, a histogram of total wishbone events vs. beta energy, fit to the theoretical beta spectrum modified by the aCORN momentum acceptances. Bottom: Fit residuals (data – fit). Error bars are statistical uncertainty.

allowed to vary in the fit: the energy calibration linear slope and offset, a vertical scale factor, and the energy resolution width factor. Thus the energy scale was determined to a relative precision of 0.5%.

The wishbone asymmetry $X(E)$ was calculated in the energy range 100–360 keV. Events with electron energy below 100 keV are problematic because: 1) the beta spectrometer was designed such that all electrons above 100 keV will strike the active scintillator, lower energy electrons may miss which complicates the calculation of $f_a(E)$; 2) the maximum transverse momentum acceptance of electrons corresponds to kinetic energy about 80 keV, so accepted low energy electrons can have axial momenta close to zero; and 3) the background is much higher at low energy. For electron energies above 360 keV the wishbone branches overlap and it is difficult to measure the asymmetry reliably.

If the neutron beam is spin-polarized, the neutrino asymmetry (B coefficient) in equation 1 contributes another term that adds to the wishbone asymmetry: $X(E) = af_a(E) \pm PBf_B(E)$ (omitting the small corrections), where P is the neutron polarization and $f_B(E)$ is a geometric function associated with the neutrino asymmetry. The positive (negative) sign

applies when the axial magnetic field direction is toward the proton (electron) detector, *i.e.* up or down. The B coefficient and $f_B(E)$ are relatively large so aCORN is very sensitive to neutron polarization. The NG-6 beam is nominally unpolarized, but the neutron guide wall is magnetic (^{58}Ni) so the superconducting magnets in its vicinity could cause a slight unwanted neutron polarization. Unfortunately we were unable to directly measure the polarization on NG-6. We collected data with both directions of the axial magnetic field. A simple average of the a coefficients obtained with magnetic field up (a_{up}) and down (a_{down}) cancels the polarization effect, assuming that $P_{\text{up}} = P_{\text{down}}$.

Figure 4 shows the measured wishbone asymmetry $X(E)$ for the full data set for each magnetic field direction. Open circles are uncorrected data. Solid circles include the calculated energy-dependent corrections for $\delta_1(E)$ and $\delta_2(E)$, and also the energy-dependent systematic corrections for the electrostatic mirror, proton soft threshold, and electron energy loss in the grid wires. Error bars are statistical. Also shown is the function $f_a(E)$ multiplied by the best-fit value of the a coefficient for each field direction. A neutron beam polarization of $P \approx 0.006$ would be sufficient to explain the observed difference, and we believe that is the cause, as the difference does not correlate with any other experimental conditions during the run. Therefore we take the simple average and obtain $a_{\text{ave}} = -0.1086 \pm 0.0030$ (statistical uncertainty).

Table I lists the significant systematic corrections and uncertainties. The largest correction was due to transverse electric fields in the electrostatic mirror, associated with the fine wire grid at the top, and field leakage near the edges at the top. A full 3D COMSOL [27] model of the electrostatic mirror was developed to calculate a correction with a relative estimated uncertainty of 20%. The PIXIE-16 threshold function on the proton signal was measured to be linear over a small range of proton energy, discarding 1.1 % of events at the low-energy side of the proton peak and producing a small false asymmetry. The largest systematic uncertainty was associated with electron scattering. Beta electrons that scatter from any material, in particular the electron collimator, or backscatter from the beta spectrometer energy detector and are not vetoed, contribute to a low-energy tail in the electron response function. Such events tend to fill in the gap between the wishbone branches and also cause a positive false asymmetry. Our best measure of this effect was a careful comparison of the data and the Monte Carlo wishbones – scattered electrons would contribute to an excess of events in the kinematically forbidden region of the wishbone gap. No evi-

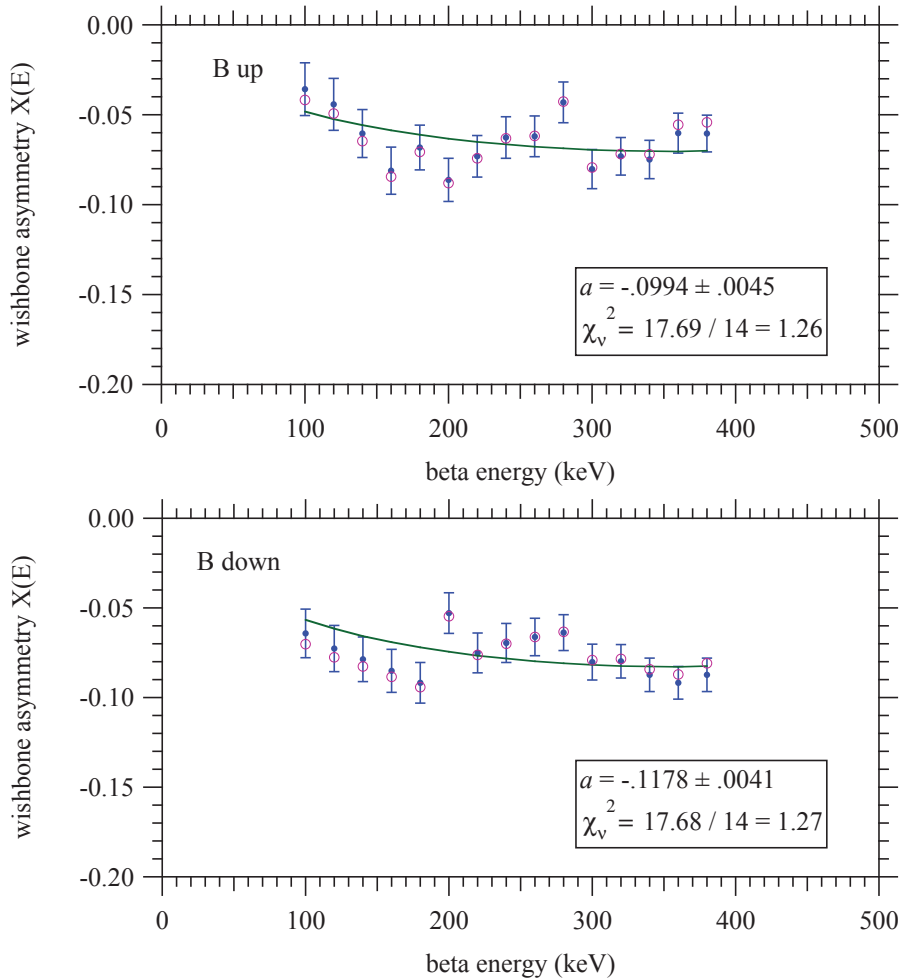


FIG. 4. Open circles: The measured, uncorrected, wishbone asymmetry $X(E)$ for each magnetic field direction. Solid points: The same data including the corrections $\delta_1(E)$, $\delta_2(E)$, and the energy-dependent systematic corrections. Error bars are statistical uncertainty. Solid curves: The product $a f_a(E)$, where a is the best fit value of the a coefficient in each case.

dence for such an excess was found, but the statistical 1σ upper limit was fairly large due to the background subtraction, corresponding to a relative 2.8 % false asymmetry, giving a correction of (1.4 ± 1.4) %. The neutron beam polarization was not measured, but we deduced a value of $P \approx 0.006$ from the data as discussed. In taking the simple average of the measured a_{up} and a_{down} , we assumed $P_{\text{up}} = P_{\text{down}}$. Due to the symmetry of the aCORN magnet and nearby magnetic materials (*e.g.* steel shield walls), we expect this to be approximately true, but to be conservative, if we allow P_{up} and P_{down} to differ by as

TABLE I. A summary of systematic corrections and uncertainties. The first three rows were applied as energy dependent corrections directly to the measured wishbone asymmetry $X(E)$. The remaining were added to the a coefficient after fitting. The second column lists the absolute uncertainties and the third column is relative to our final result for $|a|$. The total uncertainty is the quadrature sum of statistical and systematic.

	correction	1 σ uncert.	relative
electrostatic mirror	0.00571	0.00114	0.0105
proton threshold	-0.00318	0.00076	0.0070
energy loss in grid	-0.00111	0.00022	0.0020
absolute B field	-0.00010	0.00050	0.0046
B field shape	0.00031	0.00082	0.0075
residual gas	0.00046	0.00046	0.0042
e scattering	-0.00153	0.00153	0.0140
beta energy calibration		0.00031	0.0028
proton collimator align.		0.00050	0.0046
p scattering	0.00041	0.00050	0.0046
p focusing	0.00010	0.00010	0.0009
wishbone asymmetry		0.00100	0.0091
beam polarization		0.00102	0.0094
total systematic	0.00107	0.00283	0.0260
statistical		0.00302	0.0277
total uncertainty		0.00414	0.0380

much as 20 % we obtain the systematic uncertainty in the a coefficient of 0.94 % given in Table I. More details on all sources of systematic error and estimated uncertainties listed in Table I can be found in [21, 25]. The first three systematic corrections in Table I are already included in a_{ave} as energy-dependent corrections. Adding to this the remaining corrections our result is $a = -0.1090 \pm 0.0030(\text{stat}) \pm 0.0028(\text{sys})$. The quadrature sum of statistical and systematic uncertainties is $\sigma_a = 0.0041$, a 3.8 % relative uncertainty. Using equation 2 we obtain: $\lambda = -1.284 \pm 0.014$, in good agreement with the accepted value [7].

In 2014, aCORN was relocated to the new high flux neutron beamline NG-C, where data were collected from 2015–2016. We expect the experiment will achieve an ultimate uncertainty of about 1 % in the a -coefficient.

This work was supported by the National Science Foundation, U.S. Department of Energy Office of Science, and NIST (US Department of Commerce). We thank the NCNR for providing the neutron facilities used in this work, and for technical support, especially Eli Baltic, George Baltic, and the NCNR Research Facilities Operations Group.

* visiting scientist, permanent address: Korea Research Institute of Standards and Science, Daejeon, 34113, Korea.

- [1] J. S. Nico and W. M. Snow, *Annu. Rev. Nucl. Part. Sci.* **55**, 27 (2005).
- [2] H. Abele, *Prog. Part. Nucl. Phys.* **60**, 1 (2008).
- [3] D. Dubbers, *Nucl. Phys.* **A527**, 239c (1991).
- [4] J. D. Jackson, S. B. Treiman, and H. W. Wyld, *Nuclear Physics* **4**, 206 (1957).
- [5] F. Bloch and C. Møller, *Nature* **136**, 911 (1935).
- [6] J. S. Allen, *et al.*, *Phys. Rev.* **116**, 134 (1959).
- [7] C. Patrignani, *et al.* (Particle Data Group), *Chin. Phys. C* **40**, 100001 (2016).
- [8] D. Mund, *et al.*, *Phys. Rev. Lett.* **110**, 172502 (2013).
- [9] M. P. Mendenhall, *et al.*, *Phys. Rev. C* **87**, 032501(R) (2013).
- [10] T. D. Lee and C. N. Yang, *Phys. Rev.* **104**, 254 (1956).
- [11] F. E. Wietfeldt, *Mod. Phys. Lett. A* **20**, 1783 (2005).
- [12] N. Severijns and M. Beck, *Rev. Mod. Phys.* **78**, 991 (2006).
- [13] S. Gardner and C. Zhang, *Phys. Rev. Lett.* **86**, 5666 (2001).
- [14] V. K. Grigor'ev, A. P. Grishen, V. V. Vladimirkii, E. S. Nikolaevskii, and D. P. Zharkov, *Sov. J. Nucl. Phys.* **6**, 239 (1968).
- [15] C. Stratowa, R. Dobrozemsky, and P. Weinzierl, *Phys. Rev. D* **18**, 3970 (1978).
- [16] J. Byrne *et al.*, *J. Phys. G* **28**, 1325 (2002).
- [17] S. Balashov and Yu. Mostovoy, Russian Research Center Kurchatov Institute Preprint IAE-5718 /2, Moscow (1994).
- [18] B. G. Yerozolimsky, *et al.*, arXiv:nucl-ex/0401014 (2004).

- [19] F. E. Wietfeldt *et al.*, Nucl. Instr. Meth. **A545**, 181 (2005).
- [20] F. E. Wietfeldt *et al.*, Nucl. Instr. Meth. **A611**, 207 (2009).
- [21] B. Collett *et al.*, arXiv:1701.05184, submitted to Rev. Sci. Instr. (2017).
- [22] www.ncnr.nist.gov
- [23] Polyflon, Co., Norwalk, CT, USA.
- [24] Certain trade names and company products are mentioned in the text or identified in illustrations in order to adequately specify the experimental procedure and equipment used. In no case does such identification imply recommendation or endorsement by the National Institute of Standards and Technology, nor does it imply that the products are necessarily the best available for the purpose.
- [25] T. Hassan *et al.*, arXiv:1701.04820, submitted to Nucl. Instr. Meth. A (2017).
- [26] Pixie-16, XIA, Hayward, CA, USA.
- [27] COMSOL, Inc., Burlington, MA 01803, USA (www.comsol.com).